ADVANCED THEORY AND SIMULATIONS
www.advtheorysimul.com

Stretch-Healable Molecular Nanofibers

Yanxiao Han, Michal Langer, Miroslav Medved', Michal Otyepka, and Petr Král**

Ultrastretchable nanofibers formed by covalently linked molecular flakes are introduced. Molecular dynamics simulations show that mixed coronene and perfluorocoronene molecular flakes in aqueous solutions form linear stacks having predominantly an alternating pattern. When such molecular flakes are covalently connected by short flexible molecular linkers into chains of various organizations, they can form stretchable and healable fibers with parameters dependent on humidity.

The self-assembly of various nanostructures[1] and nanoparticles[2] could be directed by solvents,[3] pH,[4] salinity,[5] temperature,[6] electric,[7] optical,[8] and magnetic fields,[9] and other parameters. Once the coarsed materials are formed, they usually stop reorganizing, with a few exceptions, for example, liquid crystals can be reorganized by electric fields.[10] In contrast, most biological systems retain their ability to reorganize during their entire lifetimes. Dynamically reorganizable and healable low-D materials can have applications in electronics, photonics, energy storage, and medicine, both in dry and wet forms.

It would be particularly appealing to synthesize highly stretchable (spider-silk-like) and possibly electrically conducting nanofibers. Such nanofibers might be based on molecular flakes formed from graphene, graphene-like structures, and other 2D materials,[11] which are covalently linked into chains. The π-conjugated flakes could form conducting fibers, with structures dependent on the chemistry of the molecular linkers and other system parameters. Such molecular nanowires could transfer electric and mechanical signals from/into cellular environments.[12]

Y. Han, M. Langer, Prof. P. Král
Department of Chemistry
University of Illinois at Chicago
Chicago, IL 60607, USA
E-mail: pkral@uic.edu
M. Langer, Dr. M. Medved', Prof. M. Otyepka
Regional Centre of Advanced Technologies and Materials
Department of Physical Chemistry
Faculty of Science
Palacký University Olomouc
tř. 17. listopadu 1192/12, 771 46 Olomouc, Czech Republic
E-mail: michal.otyepka@upol.cz

The ORCID identification number(s) for the author(s) of this article can be found under https://doi.org/10.1002/adts.202000094

DOI: 10.1002/adts.202000094

In this work, we combine classical molecular dynamics (MD) simulations with quantum electronic structure calculations to study nanofibers formed by functionalized, covalently linked, and self-assembled molecular flakes based on coronene and perfluorocoronene molecules. We examine the stability of these nanofibers and their ability to reversibly stretch and reassemble (self-heal) in bulk water and air of different humidities.

We used classical MD simulations to model systems of many coronene $C_{24}H_{12}$ (COR) and perfluorocoronene $C_{24}F_{12}$ (PER) molecules in different charge states. Their partial atomic charges (**Figure 1**) were calculated in water implicit solvent by Gaussian 09.[13] In neutral PER, highly electronegative F atoms have negative charges and neighboring C atoms have positive charges, whereas in neutral COR, less electronegative H atoms have positive charges and neighboring C atoms have negative charges. Similar charge distributions are present in benzene (C_6H_6) and hexafluorobenzene (C_6F_6), which form stable alternating stacks.[14] In the charged CORs and PERs, the charge distributions show the same trend as their neutral cases, except the inner C atoms of PERs (labeled as 1 in Figure 1).

To understand coupling of such flakes, we calculated their coupling energies in vacuum by different methods (Experimental Section). The benchmarking of coupling energies calculated by selected density functional theory (DFT) methods for different molecules coupled with COR indicates that the ωB97x-D method[15] fairly reproduces the trend revealed by the reference CCSD(T)/CBS method (Figure S1 and Table S1, Supporting Information), overestimating the coupling energies by $\approx$1.6–3.8 kcal mol^{-1}. The interaction energies of the COR/PER, PER/PER, and COR/COR dimers, calculated by DFT methods, the symmetry-adapted perturbation theory (SAPT),[16] and the molecular mechanics potential (MM), are shown in Tables S2, S3 and Figure S2, Supporting Information. Under the DFT framework, the ωB97x-D and ωB97x[17] functionals with the 6-31++G(d,p) basis set were used. The interaction energies of COR/PER, PER/PER, and COR/COR dimers calculated with ωB97x-D are −37.0, −33.9, and −27.0 kcal mol^{-1}, respectively (Table S2, Supporting Information). These results are in a reasonable agreement with the SAPT0 method[18] giving the interaction energies of −48.0, −40.6, and −37.8 kcal mol^{-1} for these pairs of flakes, respectively (Table S3, Supporting Information). Figure S2b, Supporting Information, shows the decomposition of the SAPT0 interaction energies, where the dispersion interactions contribute by more than 50% to attractive energy in all three cases. Dispersion interactions originate from electron correlations, which tend to be large in unsaturated systems

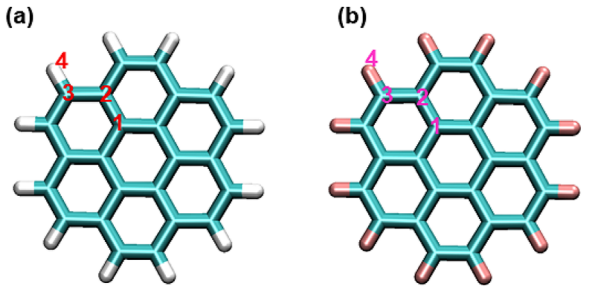

	$C_{24}H_{12}$			$C_{24}F_{12}$		
	-1 e	0 e	+1 e	-1 e	0 e	+1 e
1	-0.035	-0.021	-0.024	-0.021	0.002	0.030
2	0.177	0.176	0.138	-0.060	-0.062	-0.070
3	-0.255	-0.187	-0.151	0.100	0.172	0.204
4	0.100	0.110	0.177	-0.143	-0.142	-0.101

Figure 1. a,b) Partial charges distribution of coronene (a) and perfluorocoronene (b). Labeling of 1–4 atoms refers to the table that displays partial atomic charges used in MD simulations for negatively, neutral, and positively charged flakes.

(aromatic). Stacking of aromatic systems is known to be stabilized to a large extent by dispersion interactions, as shown in many research papers.[19] Clearly, the dispersion interactions also play a significant role in stacking and stabilization of the COR and PER flakes.[19] However, the stability of different flake dimers (CORs, PERs, and CORs/PERs dimers) is a result of a complex interplay of noncovalent interactions. Using the partial charges calculated in water implicit solvent, MM predicts somewhat smaller interaction energies, but reproduces the trend predicted by the QM methods calculated in vacuum. These energy values provide a rough physical insight about the assembling patterns observed in the MD simulations.

Free Flakes: Next, we used classical MD simulations to model the self-assembly of free molecular flakes with partial charges from Figure 1. Initially, alternating stacks of neutral CORs and PERs were simulated in water. Within 10 ns, the stacks arranged into a hexagonal lattice, as shown in **Figure 2a** and Figure S3, Supporting Information. The flakes rotated[20] and became slightly tilted, due to interactions between neighboring stacks.

In the following model simulations, all flakes were charged in the same way, each with elementary charges of +e or −e (Figure 1), but no chemical reactions of flakes with water and each other were considered. The charged flakes quickly reorganized, as shown in Figure 2b (negative) and Figure 2d (positive), collected after 30 ns. In the system with negative flakes, PERs formed columnar structures, but CORs were mostly free. On the other hand, in the system with positive flakes, CORs formed columnar structures, but PERs were mostly free. The presence of different structures, due to different charging, shown in Figure 2b,d is in line with Figure S4c,e, Supporting Information. Figure S4, Supporting Information, shows that columnar structures of eight CORs can be maintained when CORs are neutral or positively charged. Neutral PER stacks are dimerized (Figure S4d, Supporting Information), but negative PER (Figure S4e, Supporting Information) and alternating neutral COR/PER (Figure S4g, Supporting Information) stacks are stable.

When the flakes in Figure 2b,d were discharged, they reorganized in a random way where stacks were mixed preferably in a COR/PER pattern, as shown in Figure 2c,e (as in Figure S4a,g, Supporting Information). The same system was also simulated in a 150 M NaCl aqueous solution (Figure S5, Supporting Information). Here, the columnar structures formed by charged flakes were shorter, which is attributed to screening. Our simulations show that the self-assembling of free flakes can be controlled by their composition, charging, and solvent environment.

Linked Flakes: Highly-defined "spider-silk-like fibrils" could be prepared when the molecular flakes, which tend to self-assemble, are covalently linked by short and flexible bridging molecules. To explore this possibility, we linked the neutral COR and PER (COR/PER pattern) flakes and neutral COR (COR/COR pattern) flakes by short oligomeric poly(vinyl alcohol) (PVA) chains: eight flakes were connected by 7 PVA chains, each with 5 vinyl alcohol monomeric units (—$[CH_2$—$CH(OH)]_5$—), where carbon atoms of PVA connected to carbon atoms of the flakes in the trans configurations. These short linear stacks were simulated in bulk water, in the presence of water nanodroplets (vapor), and in vacuum, as shown in **Figure 3** and Figure S6, Supporting Information.

Stacks of linked neutral CORs and CORs/PERs were first prepared and stabilized for 30 ns in vacuum. Then, these stacks were placed in bulk water, close to nanodroplets, or left in a vacuum (Figure 3a and Figure S6a, Supporting Information). In these media, the stacks were gradually stretched by a force of $F = 200$ pN, applied to the right terminal flakes (one atom on the left terminal flakes was fixed), as shown in Figures S6a, Supporting Information. In all media, the flakes at the two ends of the chains started to unfold first. In the systems with water droplets (humidity), their surface tension caused the droplets to embrace groups of self-assembled flakes and to resist their disassembly by the stretching force. Since the applied force is large, the linked flakes stretched fast into chains. Once the force was turned off, the stretched chains started to collapse in a stepwise manner. They did not form the same structures as at the beginning (Figure 3a and Figure S6a, Supporting Information), but more random assemblies embracing water droplets (Figure 3c and Figure S6c, Supporting Information). Figure 3b shows some intermediate steps of stretching and collapsing (healing) nanofibers in different media.

Figure 4 shows time-dependent lengths of the above nanofibers, which were stretched by a force of $F = 200$ pN and then spontaneously released (no force). In bulk water (Figure 4a), the CORs and CORs/PERs stacks were stretched to full lengths within 1.5 ns, with relatively smooth trajectories, where the featured conformations are shown in the plots. When the force was turned off, the structures collapsed in ≈ 4 ns. In the presence of water droplets (Figure 4b,c), the droplets release in a stepwise manner the assembled flakes solvated in their interior, which led to a slow stepwise stretching of the fibers. The stronger the flakes bind to water, the more significant is this effect. For larger droplets (Figure 4b), a full stretching of the CORs and CORs/PERs stacks took 12.5 and 53 ns, respectively, when the CORs/PERs trajectory developed five plateaus. For smaller droplets (Figure 4c), the CORs and CORs/PERs

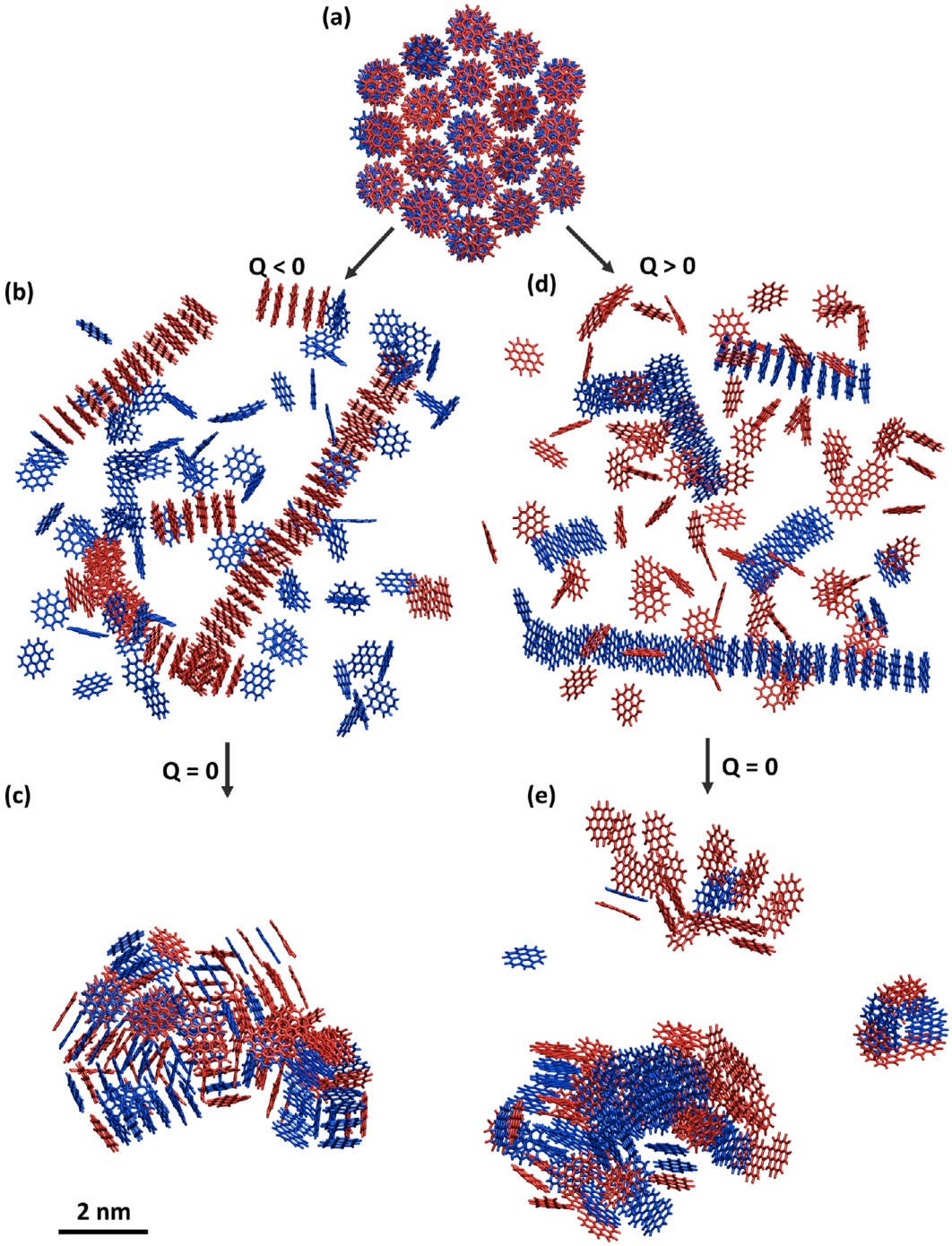

Figure 2. MD simulation snapshots showing differently stacked CORs (blue) and PERs (red) in water with NaCl counterions. a) Initially pre-assembled and thermalized system after 10 ns of simulations. b,d) Then, the flakes in (a) were negatively and positively charged by −e or +e according to Figure 1. After 30 ns simulations, the flakes reorganized differently. c,e) Then, the flakes in (b,d) were discharged. After another 30 ns, they reassembled into structures with mixed CORs and PERs. For clarity, water and ions are not displayed.

stacks were fully stretched within 5.0 and 2.5 ns, respectively. In vacuum (Figure 4d), the stretching processes took <0.2 ns. Here, CORs (binding energy of −27.0 kcal/mol) stretch faster than CORs/PERs (−37.0 kcal/mol) in bulk water and vacuum, since the mixed flakes have a stronger coupling (Figure S2 and Tables S1, S2, Supporting Information). In all simulated systems, except bulk water (slow diffusion), the structures collapsed extremely fast (<0.03 ns).

Figure 5 also shows the stretching dynamics of nanofibers in bulk water under different forces applied to their two ends.

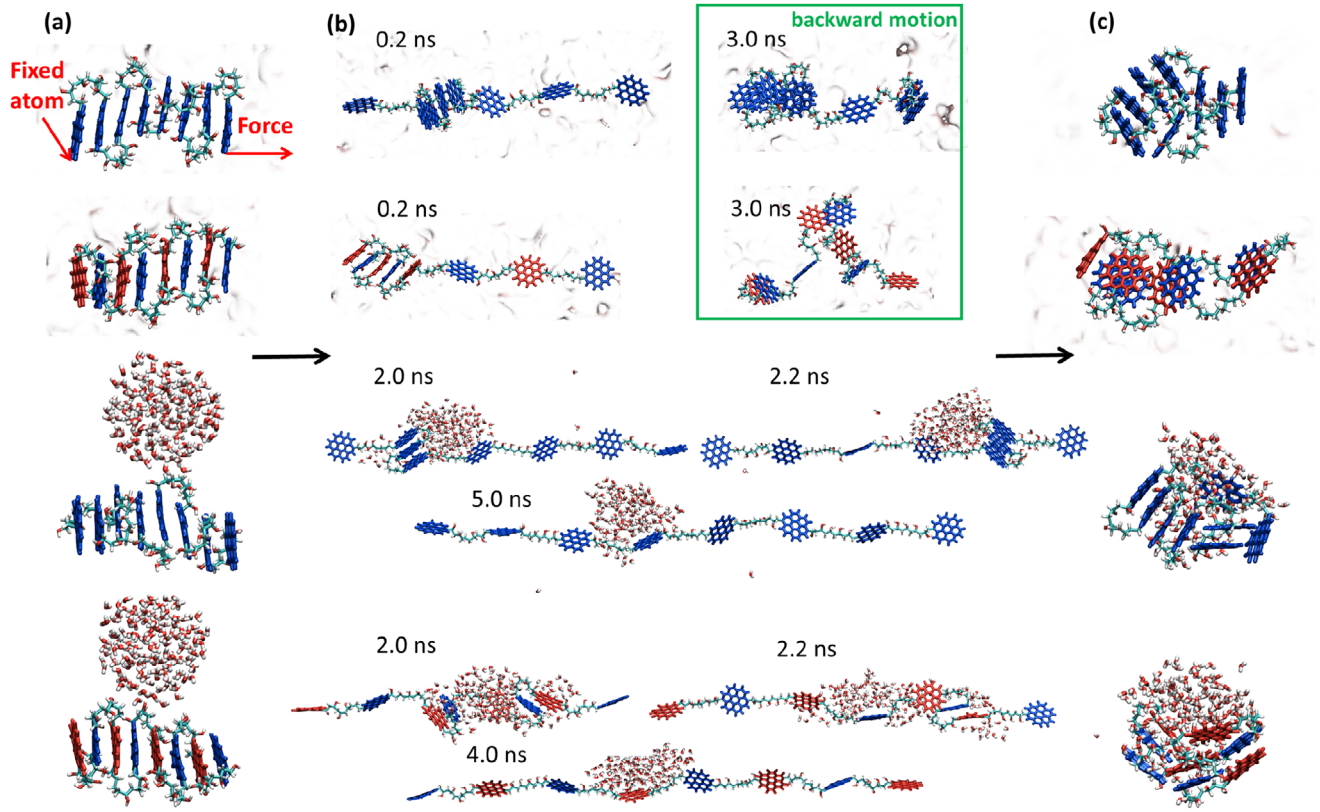

Figure 3. a) COR and COR/PER flakes linked and pre-assembled into linear stacks in bulk water and with small water droplet (top to bottom). b) Intermediate and fully stretched chains; top four panels at 0.2 ns (forward motion) and 3.0 ns (backward motion, marked in the green box). c) Re-assembled structures. Coloring scheme: blue—CORs; red—PERs.

At $F = 100$ pN, a full stretching of CORs and CORs/PERs took 25 and 12 ns, respectively (Figure 5a), while at $F = 200$ pN, it took just 0.9 and 1.2 ns (Figure 5b). The CORs were stretched faster than PERs during earlier stretching times, as shown in Figure 5a,b, which is in line with cases in Figure 4a–d. However, the overall stretching time is affected by fluctuations. In general, at smaller stretching forces, the prolongation was slow with typical steps, while at larger forces it was fast and smooth. The steps are caused by energy barriers associated with the disassembly of individual flakes from the stacks. Larger forces can easily overcome these barriers, giving fast and smooth prolongation of the nanofibers.

To better understand the fluctuations in elongation of these nanofibers during their stretching, three separate replicas of neutral CORs and CORs/PERs fibers were separately stretched in bulk water by a force of 85 pN. As shown in Figure 5c,d, the elongation steps and simulation times that were necessary for these nanofibers to fully stretch were slightly different in the three replicas. These differences may be related to slightly different initial arrangements of the structures and fluctuations present in each replica. However, these effects should average out in ensembles of such fibers, that is, in longer fibers or many parallel fibers.

In summary, using MD simulations and electronic structure methods, we have shown that coronene and perfluorocoronene molecules can self-assemble into stacks in environments of different humidities. When the molecular flakes within such stacks are covalently linked, they can form stretchable and healable nanofibers.[25] These ultrastretchable and possibly electrically conducting nanofibers can have many diverse applications in materials, electronics, and sensing.

Computational Details

In the MD simulations, the partial atomic charges of flakes with different charges (−1, +1, and 0) were derived using the RESP method at the MP2/6-31G* level by Gaussian 09[13] in water implicit solvent. The systems of free and linked stacked flakes were simulated by NAMD[21] and the CHARMM general force field.[22] The PME method was used for the evaluation of long-range Coulomb interactions. The time step was set to 2 fs. The simulations were performed in the NpT ensemble ($p = 1$ bar and $T = 298$ K), using the Langevin dynamics with a damping constant of 1 ps^{-1}.

To gain more physical insight into the coupling of CORs and PERs dimers, the coupling energies were calculated by DFT and SAPT methods on dimers optimized in vacuum (see Supporting Information). The dimers and monomers were first optimized at the ωB97x-D/6-31++G(d,p) level of theory, which was followed by single-point calculations with ωB97x-D and ωB97x functionals with the 6-31++G(d,p) basis set (Gaussian09). The SAPT0 and sSAPT0[23] (i.e., modified SAPT0 method with empirically scaled exchange terms evaluated in S^2 approximation) calculations were performed in the Psi4 code[24] with the aug-cc-pVDZ basis set, on the previously optimized geometries.

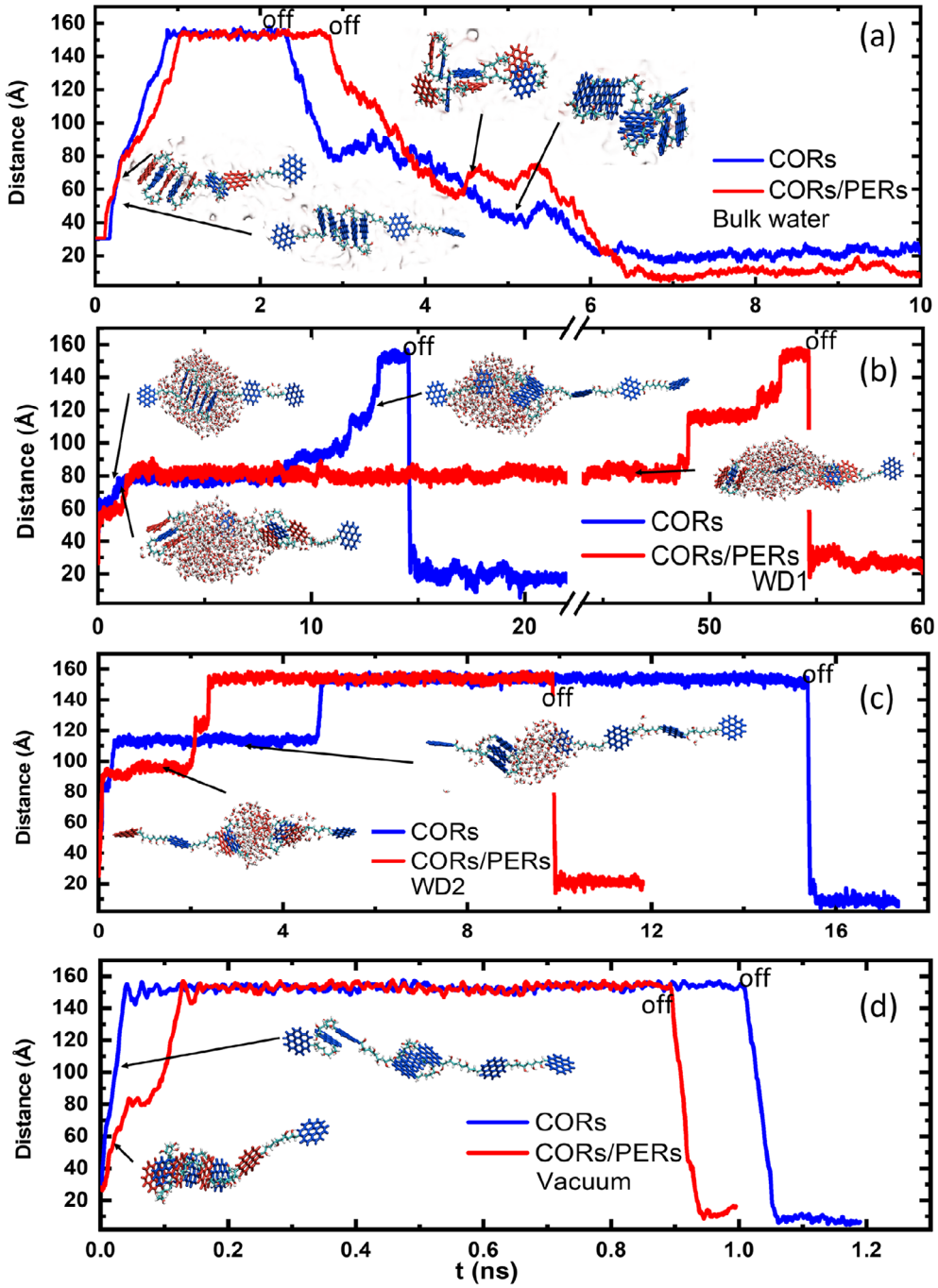

Figure 4. Stretching of neutral CORs and neutral CORs/PERs fibers. a–d) The distance between the two fiber ends under a stretching force of $F = 200$ pN: a) in bulk water, b) with a big water droplet, c) with a small water droplet, and d) in vacuum. The force is turned off at times when the chain lengths are seen to drop from their maximum values (marked as off). Coloring scheme: blue—CORs; red—PERs.

The MM interaction energies were calculated by the NAMD energy plugin, which evaluates Coulombic and Lennard-Jones (LJ) 6–12 potential energy contributions. The two adjacent flakes in the middle of the columnar structures (Figure S4a,d,g, Supporting Information) were selected as the interacting CORs, PERs, and CORs/PERs dimers. The MM energies were averaged over the last 2 ns (50 frames). The parameters in the potentials were taken from the CHARMM general force field with charges calculated as in Figure 1. The dielectric constant was set to 1.

Supporting Information

Supporting Information is available from the Wiley Online Library or from the author.

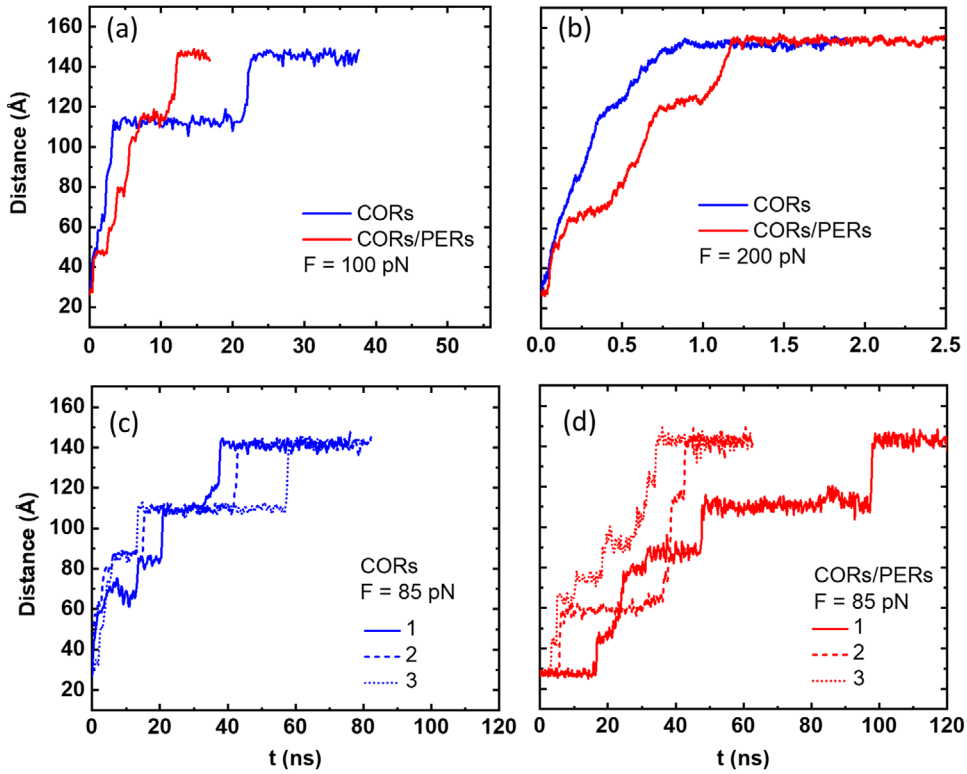

Figure 5. a,b)Stretching of neutral COR and COR/PER nanofibers in bulk water: The lengths of nanofibers under stretching forces of $F = 100$ pN (a) and 200 pN (b). c,d) Three replicas stretched separately with a force of 85 pN: c) neutral CORs, d) neutral CORs/PERs.

Acknowledgements

Y.H. and M.L. contributed equally to this work. M.L. acknowledges the support from the Internal Student Grant Agency of the Palacký University in Olomouc, Czech Republic (IGA_PrF_2020_022), the support from the ERC (project No. 683024 from the European Union's Horizon 2020), and the support from Ministry of Education, Youth and Sports (grant number: CZ.02.1.01/0.0/0.0/16_019/0000754). Y.H. acknowledges the support from the Dean's Scholar Fellowship (UIC).

Conflict of Interest

The authors declare no conflict of interest.

Keywords

molecular dynamics simulations, molecular nanofibers, self-assembly, stretch-healable fibers

Received: April 30, 2020
Revised: July 15, 2020
Published online:

[1] a) N. Patra, B. Wang, P. Král, *Nano Lett.* **2009**, *9*, 3766; b) N. Patra, Y. Song, P. Král, *ACS Nano* **2011**, *5*, 1798; c) E. Cohen, H. Weissman, I. Pinkas, E. Shimoni, P. Rehak, P. Král, B. Rybtchinski, *ACS Nano* **2018**, *12*, 317.

[2] M. Grzelczak, L. M. Liz-Marz an, R. Klajn, *Chem. Soc. Rev.* **2019**, *48*, 1342.

[3] P. A. Korevaar, C. Schaefer, T. F. A. de Greef, E. W. Meijer, *J. Am. Chem. Soc.* **2012**, *134*, 13482.

[4] M. Yang, H. Chan, G. Zhao, J. H. Bahng, P. Zhang, P. Král, N. A. Kotov, *Nat. Chem.* **2017**, *9*, 287.

[5] R. J. Stover, A. K. Murthy, G. D. Nie, S. Gourisankar, B. J. Dear, T. M. Truskett, K. V. Sokolov, K. P. Johnston, *J. Phys. Chem. C* **2014**, *118*, 14291.

[6] M. Grzelczak, J. Vermant, E. M. Furst, L. M. Liz-Marzán, *ACS Nano* **2010**, *4*, 3591.

[7] M. K. Bera, H. Chan, D. F. Moyano, H. Yu, S. Tatur, D. Amoanu, W. Bu, V. M. Rotello, M. Meron, P. Král, B. Lin, M. L. Schlossman, *Nano Lett.* **2014**, *14*, 6816.

[8] H. Zhao, S. Sen, T. Udayabhaskararao, M. Sawczyk, K. Kucanda, D. Manna, P. K. Kundu, J. W. Lee, P. Král, R. Klajn, *Nat. Nanotechnol.* **2016**, *11*, 82.

[9] G. Singh, H. Chan, A. Baskin, E. Gelman, N. Repnin, P. Král, R. Klajn, *Science* **2014**, *345*, 1149.

[10] D. Miyajima, K. Tashiro, F. Araoka, H. Takezoe, J. Kim, K. Kato, M. Takata, T. Aida, *J. Am. Chem. Soc.* **2009**, *131*, 44.

[11] A. K. Geim, I. V. Grigorieva, *Nature* **2013**, *499*, 419.

[12] a) A. V. Titov, P. Král, R. Pearson, *ACS Nano* **2010**, *4*, 229; b) L. Camilli, M. Passacantando, *Chemosensors* **2018**, *6*, 1; c) D. J. Lipomi, M. Vosgueritchian, B. C. K. Tee, S. L. Hellstrom, J. A. Lee, C. H. Fox, Z. Bao, *Nat. Nanotechnol.* **2011**, *6*, 788.

[13] M. J. Frisch, G. W. Trucks, H. B. Schlegel, G. E. Scuseria, M. A. Robb, J. R. Cheeseman, G. Scalmani, V. Barone, G. A. Petersson, H. Nakatsuji, X. Li, M. Caricato, A. Marenich, J. Bloino, B. G. Janesko, R. Gomperts, B. Mennucci, H. P. Hratchian, J. V. Ortiz, A. F. Izmaylov, J. L. Sonnenberg, D. Williams-Young, F. Ding, F. Lipparini, F. Egidi, J. Goings, B.

Peng, A. Petrone, T. Henderson, D. Ranasinghe, V. G. Zakrzewski, J. Gao, N. Rega, G. Zheng, W. Liang, M. Hada, M. Ehara, K. Toyota, R. Fukuda, J. Hasegawa, M. Ishida, T. Nakajima, Y. Honda, O. Kitao, H. Nakai, T. Vreven, K. Throssell, J. A. Montgomery, Jr., J. E. Peralta, F. Ogliaro, M. Bearpark, J. J. Heyd, E. Brothers, K. N. Kudin, V. N. Staroverov, T. Keith, R. Kobayashi, J. Normand, K. Raghavachari, A. Rendell, J. C. Burant, S. S. Iyengar, J. Tomasi, M. Cossi, J. M. Millam, M. Klene, C. Adamo, R. Cammi, J. W. Ochterski, R. L. Martin, K. Morokuma, O. Farkas, J. B. Foresman, D. J. Fox, *Gaussian 09, Revision A.02*, Gaussian, Inc., Wallingford CT, USA **2016**.

[14] a) S. Tsuzuki, T. Uchimaru, M. Mikami, *J. Phys. Chem. A* **2006**, *110*, 2027; b) J. H. Williams, J. K. Cockcroft, A. N. Fitch, *Angew. Chem. Int. Ed.* **1992**, *31*, 1655; c) C. J. Pace, J. Gao, *Acc. Chem. Res.* **2013**, *46*, 907.

[15] J. D. Chai, M. Head-Gordon, *Phys. Chem. Chem. Phys.* **2008**, *10*, 6615.

[16] G. Chalasinski, M. M. Szczesniak, *Chem. Rev.* **1994**, *94*, 1723.

[17] J. D. Chai, M. Head-Gordon, *J. Chem. Phys.* **2008**, *128*, 084106.

[18] B. Jeziorski, R. Moszynski, K. Szalewicz, *Chem. Rev.* **1994**, *94*, 1887.

[19] a) K. E. Riley, P. Hobza, *Acc. Chem. Res.* **2013**, *46*, 927; b) J. Hwang, B. E. Dial, P. Li, M. E. Kozik, M. D. Smitha, K. D. Shimizu, *Chem. Sci.* **2015**, *6*, 4358; c) J. C. Sancho-García, A. J. Pérez-Jiménez, *J. Chem. Phys.* **2014**, *141*, 134708.

[20] M. Paloncýová, M. Langer, M. Otyepka, *J. Chem. Theory Comput.* **2018**, *14*, 2076.

[21] J. C. Phillips, R. Braun, W. Wang, J. Gumbart, E. Tajkhorshid, E. Villa, C. Chipot, R. D. Skeel, L. Kalé, K. Schulten, *J. Comput. Chem.* **2005**, *26*, 1781.

[22] K. Vanommeslaeghe, A. D. MacKerell, *J. Chem. Inf. Model.* **2012**, *52*, 3144.

[23] T. M. Parker, L. A. Burns, R. M. Parrish, A. G. Ryno, C. D. Sherrill, *J. Chem. Phys.* **2014**, *140*, 094106.

[24] R. M. Parrish, L. A. Burns, D. G. A. Smith, A. C. Simmonett, A. E. DePrince, E. G. Hohenstein, U. Bozkaya, A. Y. Sokolov, R. Di Remigio, R. M. Richard, *J. Chem. Theory Comput.* **2017**, *13*, 3185.

[25] S. Wang, M. W. Urban, *Nat. Rev. Mater.* **2020**, *5*, 562.